Triangular lattice antiferromagnet $RbFe(MoO_4)_2$ in high magnetic fields

A. I. Smirnov,[1] H. Yashiro,[2] S. Kimura,[2] M. Hagiwara,[2] Y. Narumi,[3] K. Kindo,[3] A. Kikkawa,[4] K. Katsumata,[4] A. Ya. Shapiro,[5] and L. N. Demianets[5]

[1]*P. L. Kapitza Institute for Physical Problems, RAS, 119334 Moscow, Russia*

[2]*Center for Quantum Science and Technology under Extreme Conditions (KYOKUGEN), Osaka University, 1-3 Machikaneyama, Toyonaka, Osaka 560-8531, Japan*

[3]*Institute for Solid State Physics (ISSP), University of Tokyo, 5-1-5 Kashiwanoha, Kashiwa, Chiba 277-8581, Japan*

[4]*RIKEN SPring-8 Center, Harima Institute, Sayo, Hyogo 679-5148, Japan*

[5]*A. V. Shubnikov Institute for Crystallography, RAS, 117333 Moscow, Russia*

(Received 5 September 2006; revised manuscript received 29 January 2007; published 13 April 2007)

The saturation of magnetization was studied in pulsed magnetic fields (H) for the triangular lattice antiferromagnet $RbFe(MoO_4)_2$ at temperatures (T) below the magnetic ordering point T_N. The field-driven transition from the antiferromagnetic to the paramagnetic phase was studied by specific-heat measurements in a steady magnetic field. The specific heat shows a sharp peak at a value of the magnetic field below which a singularity in the magnetization curve occurs, indicating a splitting of the field-induced transition to the paramagnetic phase. This splitting vanishes at low temperatures. A complete T-H phase diagram is derived experimentally both for the magnetic field lying in the spin plane and perpendicular to the plane. A spin-flip magnetic-resonance mode with the softening of the spin-wave spectrum at the saturation field has been observed. The gap of the spin-wave spectrum was found to be reduced by zero-point fluctuations by a factor of 0.82 ± 0.08 with respect to the prediction of the molecular-field theory.

DOI: 10.1103/PhysRevB.75.134412 PACS number(s): 75.50.Ee, 76.50.+g, 75.30.Cr, 75.60.Ej

I. INTRODUCTION

Classical spins placed on a regular two-dimensional triangular lattice have a 120° spin structure in zero field. They exhibit a set of field- and temperature-driven phase transitions between magnetic phases of different kinds of order parameter and universality classes. Some of these phases attract attention due to the chiral degree of freedom, while other phases are stabilized by thermal or quantum fluctuations. The problem of a two-dimensional (2D) antiferromagnet on a triangular lattice (AFMTL) was extensively studied both theoretically (see, e.g., Refs. 1–7) and experimentally (see, e.g., Refs. 8–13).

$RbFe(MoO_4)_2$ appears to be a rare example of a quasi-2D antiferromagnet on a triangular lattice. Fe^{3+} ions having the spin $S=5/2$ form magnetic layers with a regular triangular lattice. The layers are separated by nonmagnetic Rb ions and MoO_4 complexes (see the crystal structure in, e.g., Ref. 14). This compound has a moderate exchange field, which enables one to follow experimentally all the field-driven transformations of the spin structure, including the saturation of the magnetization. The magnetization curve marking a 2D triangular lattice antiferromagnet was first reported for powder samples.[9] The curve exhibited a characteristic plateaulike behavior at the level of $1/3M_{sat}$, where M_{sat} is the saturation magnetization. Detailed investigations of magnetic and thermodynamic properties, resonance spectra, and phase transitions of single crystals were performed in Refs. 10–12. The zero-field structure of the 120° type was confirmed by a neutron-scattering study.[15] The most fundamental points were the study of the plateaulike phase, which exists due to fluctuations and the derivation of the T-H phase diagram. $RbFe(MoO_4)_2$ was studied in detail in the low- and intermediate-field ranges, but the upper critical field of the antiferromagnetic phase has still not been studied systematically.

In this paper, we describe the high-magnetic-field properties of single-crystal samples of $RbFe(MoO_4)_2$. A pulsed magnet was used for magnetization measurements up to 50 T. Specific-heat and high-frequency electron-spin-resonance (ESR) measurements were taken in a steady field up to 14 T.

These measurements have two main results: the complete T-H phase diagram of the quasi-2D antiferromagnet on the regular triangular lattice and observation of the splitting of the field-induced transition to the paramagnetic phase.

II. EXPERIMENTAL PROCEDURE

Single-crystal samples of $RbFe(MoO_4)_2$ from the same batch as in Ref. 12 were used. The crystals have the form of triangular plates with a thickness of about 0.7 mm and an in-plane size up to 7 mm. The C^3 crystallographic axis was oriented perpendicular to plate planes. The samples having the form of thin plates of a suitable size were cut from these crystals. The magnetization curves were measured with a pulsed 60 T magnet at KYOKUGEN in Osaka University. The specific-heat measurements in the field range 9–14 T were performed using the commercial Quantum Design physical property measurement system device at RIKEN SPring-8 Center by the "2-τ" method. The ESR spectra were taken by utilizing an ABmm-network analyzer combined with a 16 T superconducting magnet at KYOKUGEN. The 35 GHz ESR spectra in magnetic fields beyond 16 T were recorded using a transmission-type spectrometer with a pulsed magnet.

III. EXPERIMENTAL RESULTS

A typical magnetization curve of $RbFe(MoO_4)_2$ for the in-plane magnetic field is shown in Fig. 1. It demonstrates a

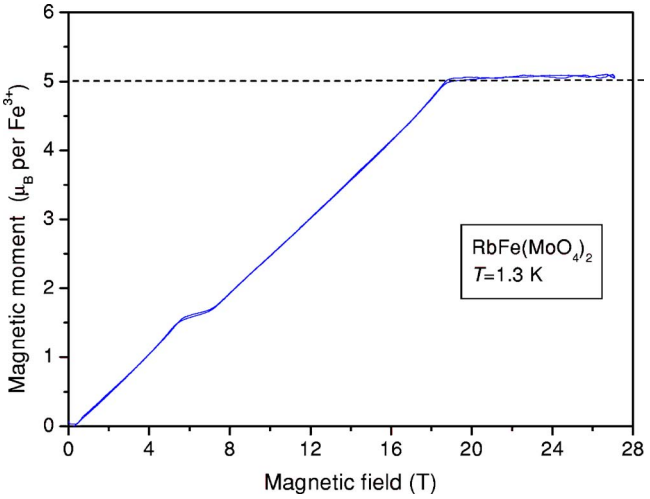

FIG. 1. (Color online) Magnetization curve of a $RbFe(MoO_4)_2$ crystal at $T=1.3$ K for $H \perp C^3$.

linear growth in the low-field range, then a plateaulike range near $\frac{1}{3}M_{sat}$. After the plateau, a linear growth is observed and finally, saturation at a magnetic field of $\mu_0 H_{sat\|} = 18.2 \pm 0.2$ T. Calibration of the magnetic moment was performed via comparison with the low-field data of Ref. 12. The maximum obtained magnetic moment coincides to within the experimental error with the expected value of 5 Bohr magnetons per Fe ion.

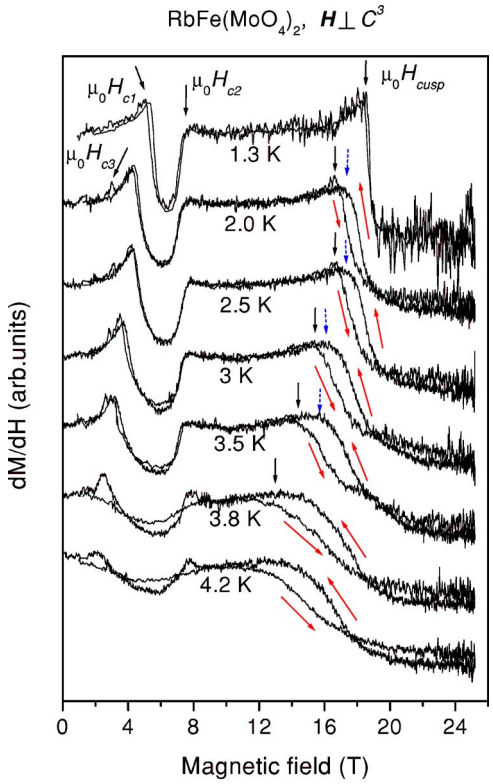

FIG. 2. (Color online) Field derivatives of the magnetization of a $RbFe(MoO_4)_2$ crystal at different temperatures for $H \perp C^3$. Solid and dashed arrows mark magnetic fields H_{cusp} for increasing and decreasing fields, respectively.

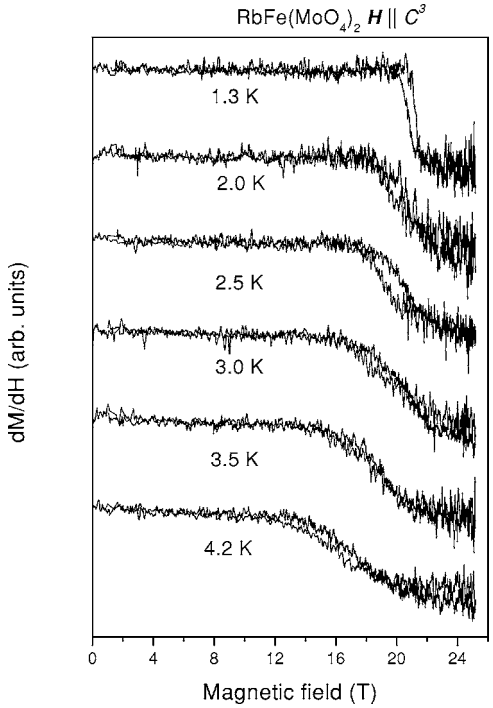

FIG. 3. Field derivatives of the magnetization of a $RbFe(MoO_4)_2$ crystal at different temperatures for $H \| C^3$.

The dM/dH curves for both principal orientations perpendicular and parallel to the C^3 axis are presented in Figs. 2 and 3. The curves on Fig. 2 clearly mark the anomalies at the beginning and the end of the plateaulike range, H_{c1} and H_{c2}, respectively. In addition, the dM/dH curves demonstrate a remarkable cusp at the saturation point. This cusp is most clearly pronounced at low temperatures and is distinguishable up to 3.5 K. With the rise of temperature, the saturation process and the aforementioned cusp become smeared and a hysteresis appears in the vicinity of the saturation. With the magnetic field directed along the C^3 axis, the cusp was not observed and the hysteresis has much smaller magnitude.

A small hysteresis in the plateaulike range visible on Figs. 1 and 2 is obviously due to the pulse technique used in this measurement, because the magnetization curves taken in steady field in the range up to 10 T in Refs. 10 and 12 show that there is no hysteresis in a quasiequilibrium process. The hysteresis observed using pulse method may arise due to the magnetocaloric effect discussed below in Sec. IV A.

The low-temperature saturation point for $H \| C^3$ occurs at a higher value of applied field of 20.2 T. Taking into account the demagnetization field of the thin plate sample with the saturation magnetization of spins $S=5/2$ placed on the Fe^{3+} sites, we derive the saturation field for this orientation to be $\mu_0 H_{sat\perp} = 19.9$ T.

For the description of the saturation process at different temperatures, we designate the magnetic field at the beginning of the saturation as the cusp field for $H \perp C^3$. For $H \| C^3$, we designate the magnetic field at the beginning of the saturation as the field H_b, where dM/dH reduces to 5% of the normal value. We also mark for both cases the field $H_{1/2}$ when the derivative dM/dH is reduced by half. The field at the beginning of the saturation and $H_{1/2}$ practically coincide

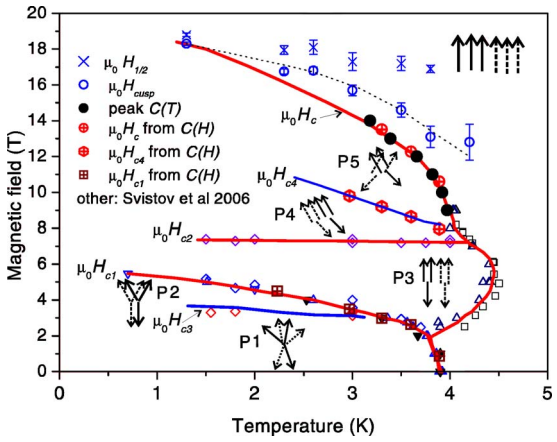

FIG. 4. (Color online) Phase diagram at $H \perp C^3$. Symbols explanation for the data of Ref. 12, taken in the field range below 9 T: △, $C(T)$ peak; ▽, $C(H)$ peak; ◇, $M(H)$ singularities; □, NMR shift.

at the lowest temperature, but separate quickly with heating. These characteristic fields are plotted in the graphs of Figs. 4 and 5. The values of H_{cusp} were determined from magnetization curves taken in increasing magnetic fields. For the decreasing field measurements, the cusp is detected only at $T \leqslant 3.0$ K, and at slightly larger field values, as may be seen in Fig. 2.

Next, we followed the field-induced transition to the paramagnetic state by observation of the singularities in the specific heat C_{mol}. The typical temperature dependences $C_{mol}(T)$ are presented in Fig. 6, and the field dependences $C_{mol}(H)$ in Fig. 7. The specific-heat data in low fields were reported earlier.[12] We see that the anomaly in the specific heat at the transition temperature T_c or the high-field anomaly of the $C_{mol}(H)$ curve in the field H_c is much more pronounced when compared to the dM/dH curves. In addition to the sharp peaks at H_c in the $C_{mol}(H)$ curves, there are also smeared peaks at the magnetic field marked as H_{c4} on Fig. 7. The fields of the specific-heat anomalies are again collected on the phase diagram in Fig. 4, where the data of the previous

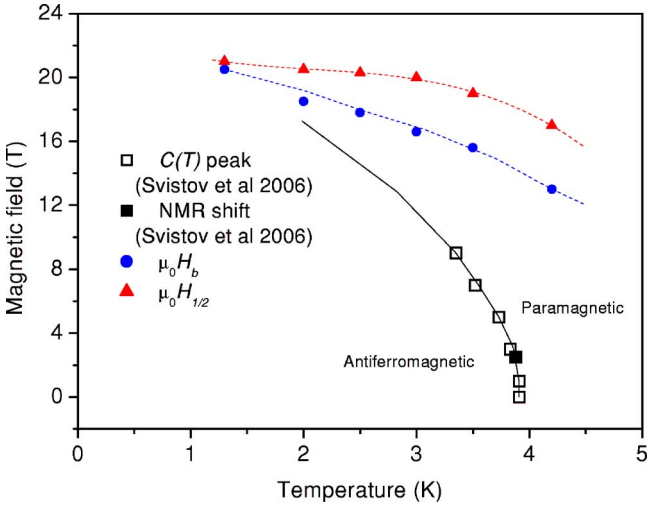

FIG. 5. (Color online) Phase diagram and characteristic fields of the magnetization process at $H \| C^3$.

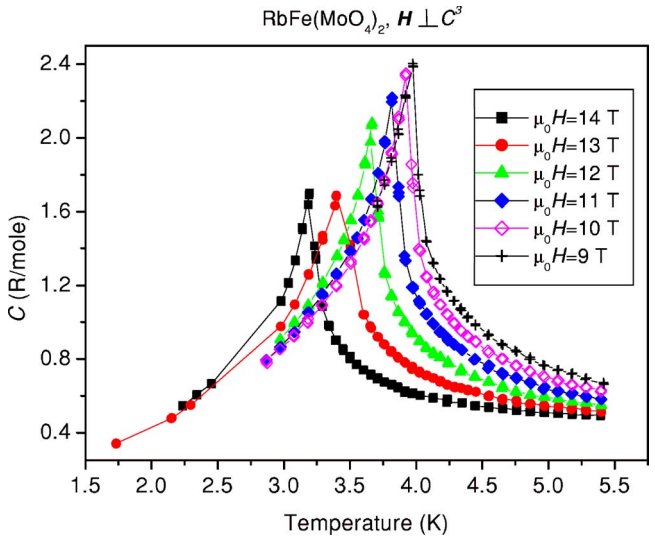

FIG. 6. (Color online) Temperature dependence of the specific heat of the $RbFe(MoO_4)_2$ crystals with $H \perp C^3$ in different magnetic fields.

work[10,12] on the specific heat and magnetization below 10 T are also presented.

Low-temperature electron-spin-resonance lines are collected on the Figs. 8 and 9, and the corresponding resonance-frequency–field dependences for different ESR modes are presented in Figs. 10 and 11, respectively. In Fig. 10, the ESR spectra consist of three intensive energy branches and an additional branch with weak absorption detected at lower frequencies in Ref. 10. Two intense modes have a gap of 90 GHz in zero field with one branch increasing and the other decreasing in frequency as a function of applied field. The upper branch was observed to be split into two close resonances. The lower branch softens at the lower plateau limit H_{c1}. The frequency of the third intensive mode, softening at the upper plateau limit H_{c2}, increases in magnetic fields above the plateaulike range, and decreases toward the

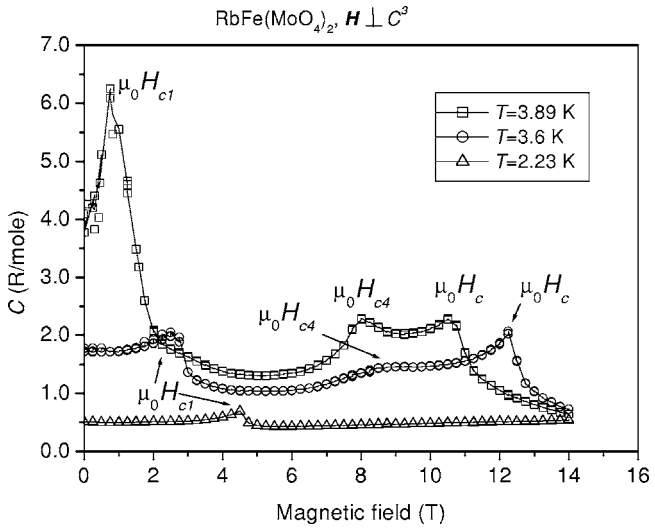

FIG. 7. Field dependence of the specific heat of the $RbFe(MoO_4)_2$ crystals at $H \perp C^3$.

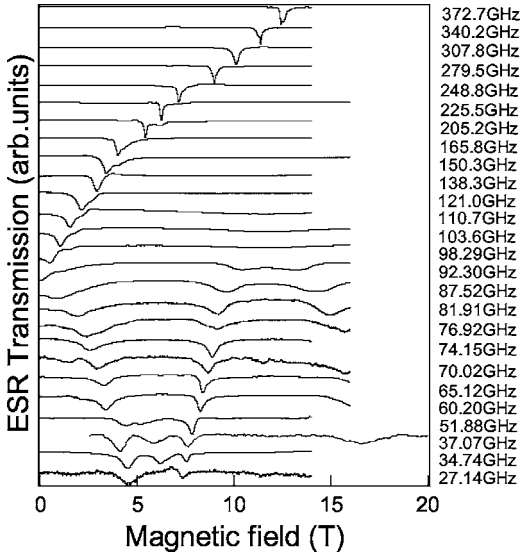

FIG. 8. ESR lines at different frequencies with $T=1.5$ K for $H \perp C^3$.

saturation field. These observations agree well with the spin-resonance modes reported in Ref. 10 for the lower-frequency range. In the high-field range (above the plateau), the evolution of the spin-resonance mode arising from zero frequency at the upper plateau boundary was traced to the saturation field $H_{sat\|}$. Here, we observed a spin-flip mode with strong softening. Figures 12(a) and 12(b) show the temperature evolution of the ESR spectra for $H \| C^3$ and $H \perp C^3$, respectively. A change in the ESR spectra at the phase transition from the ordered phase to the paramagnetic phase at $T_N=3.8$ K is clearly seen.

IV. DISCUSSION

A. Long-range and short-range ordering at finite temperatures in high magnetic fields

The spin structures for different magnetic phases of $RbFe(MoO_4)_2$, as shown on the phase diagram in Fig. 4,

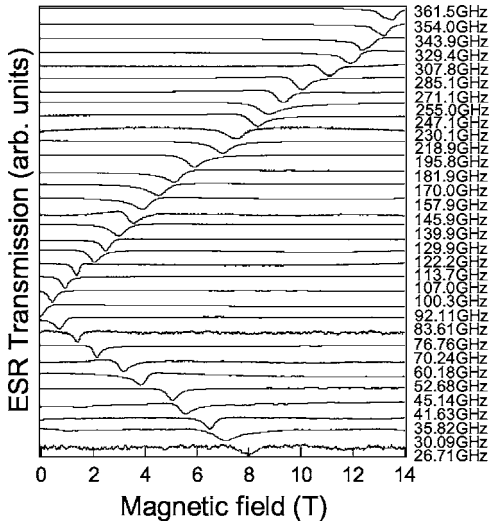

FIG. 9. ESR lines at different frequencies and $T=1.5$ K for $H \| C^3$.

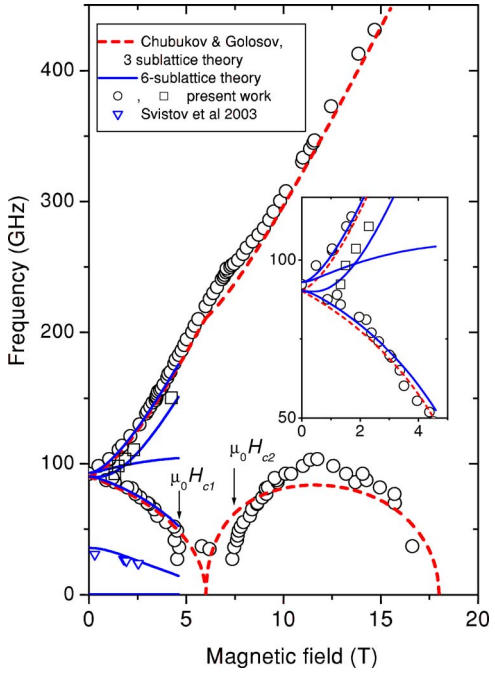

FIG. 10. (Color online) Frequency vs magnetic field dependences for ESR modes of $RbFe(MoO_4)_2$ at $H \perp C^3$, $T=1.5$ K. The dashed line represents molecular-field calculations (Ref. 5) for three sublattice model with the parameters $6JS/(g\mu_B)=6$ T and $DS/(g\mu_B)=0.57$ T, and the solid lines are the molecular-field calculations for a six sublattice model with the parameters $6JS/(g\mu_B)=6$ T, $4J'S/(g\mu_B)=0.0425$ T, and $DS/(g\mu_B)/=0.57$ T.

were proposed in Refs. 10 and 12 on the basis of the available experimental data and theoretical analysis. The solid and dashed arrows correspond to spins in two neighboring magnetic layers. The phase transitions at the magnetic fields H_{c1} and H_{c2} are the transitions into and out of the plateaulike phase, which are the intrinsic features of the 2D AFMTL. The transitions at the magnetic fields H_{c3} and H_{c4} are supposed to be associated with the change of the mutual orientation of spins in neighboring magnetic layers and are due to the weak interlayer exchange and other weak interactions. This type of transition was analyzed theoretically in Ref. 7. The change of the mutual orientation of spins in adjacent magnetic layers was indeed experimentally detected by a change of NMR spectra,[16] corresponding to a phase transition between the commensurate and incommensurate magnetic structures at the magnetic field H_{c3}.

A peculiarity of the saturation process of the planar spin structure in the $RbFe(MoO_4)_2$ (at $H \perp C^3$) is the cusp of the dM/dH at the field H_c. This cusp, of approximately the same magnitude as the one at the lower edge of the magnetization plateau H_{c1}, indicates strong spin fluctuations at the saturation point. We suppose that its nature is analogous to the cusp at the field H_{c1}, where the transition from the noncollinear to collinear "up-up-down" structure occurs. Indeed, for the field lying in the easy plane, a planar configuration of the type "a" or "b" of Fig. 13 is considered just below the saturation. These degenerate configurations imply that fluctuations are stabilizing the collinear phase, and hence, one reaches the saturation magnetization at a slightly smaller

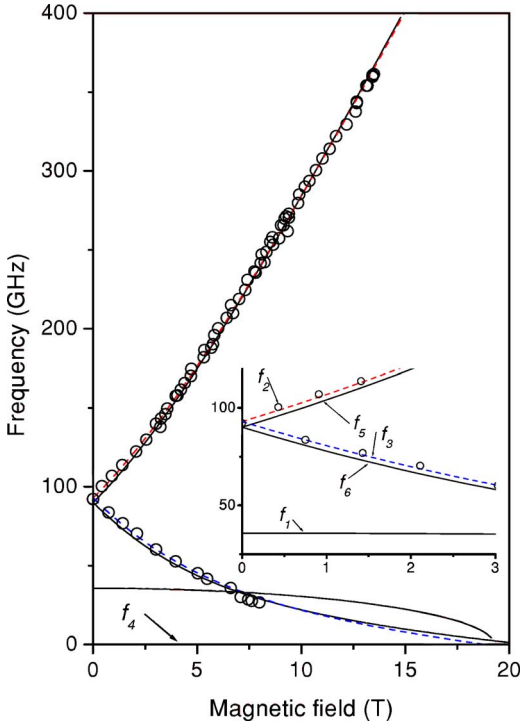

FIG. 11. (Color online) Frequency vs magnetic field dependences for ESR modes of $RbFe(MoO_4)_2$ at $H \| C^3$ and $T=1.5$ K. Solid and dashed lines represent molecular-field calculation for six sublattice model (Ref. 17) with the same parameters as in Fig. 10.

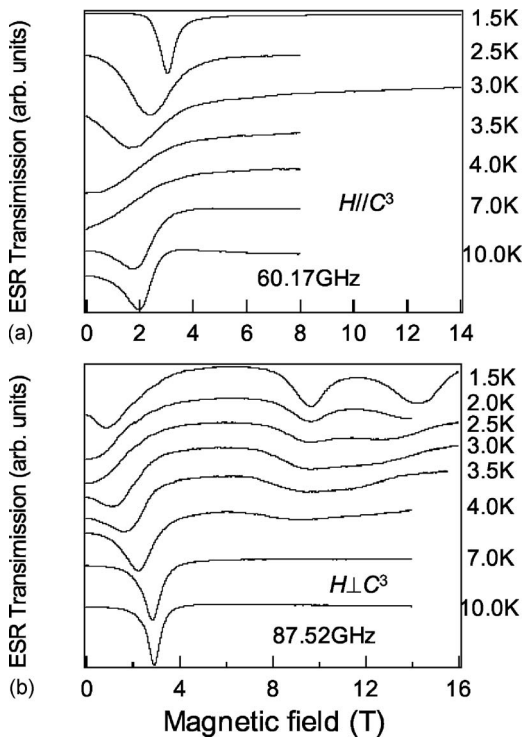

FIG. 12. ESR lines at different temperatures for (a) $H \| C^3$ and (b) $H \perp C^3$. The Néel temperature of $RbFe(MoO_4)_2$ is 3.8 K.

field than in the absence of fluctuations. This should result in an increase in the derivative dM/dH before it drops to zero.

The umbrella structure (sketch "c" in Fig. 13) takes place for $H \| C^3$. There are no degenerate spin configurations which differ for the mutual spin orientations in this case, while the rotational degeneracy corresponding to uniaxial anisotropy is usually lifted by higher-order in-plane anisotropy. Correspondingly, we do not observe a cusp in dM/dH curves for this orientation. The temperature evolution of this cusp, rising with cooling, indicates zero-point spin fluctuations, as well as the nonvanishing magnetic-field range of the plateau-like phase at the lowest temperatures.

The specific-heat measurements reveal that the destruction of long-range order detected by the sharp peak in the specific heat appears at a magnetic field H_c which is far below the field of the beginning of the saturation, H_{cusp} or H_b. The specific-heat anomaly and the cusp of dM/dH are located at well separated magnetic fields. Thus, we conclude that the field-driven transition from the antiferromagnetic to the paramagnetic phase is split into two transitions, one of them occurs at the field H_c of the specific-heat anomaly and the second transition is at field H_{cusp}.

Such behavior was predicted by Korshunov,[4] who suggested a scenario with a two-step transition from the high-field ordered phase to a paramagnetic phase for the 2D AFMTL. For the phase with the layer spin structures a or b shown in Fig. 13 (phase P5 of Fig. 4), the following evolution was suggested. At the lower critical field, the long-range order of the transverse spin components should disappear. However, the spatial correlations of the transverse components will decay by a power law for a nonzero field interval. At the higher critical field, the correlations should start decaying exponentially. The nonzero inverse correlation length marks the final critical point at the transition to a paramagnetic phase. This scenario may be responsible for the observed discrepancy between the positions of the critical anomalies in the specific heat and magnetization. This scenario implies that the magnetization should not change strongly at the first transition, which mainly conserves the transverse spin components, but should change at the high-field transition, in correspondence with our observations.

We also note that for temperatures above half of T_N, the high-field anomalies at H_c and H_b are well below $H_{1/2}$, as one can see in both phase diagrams in Figs. 4 and 5. This means that the short-range triangular antiferromagnetic order, maintained by the strong exchange interaction, exists up to much higher fields, of the order of $H_{sat}(T=0)$. Indeed, the ordering temperature of $RbFe(MoO_4)_2$ is much smaller than the absolute value of Curie-Weiss temperature[14] $\theta_{CW}=-21$ K. Thus, the strong exchange correlations should

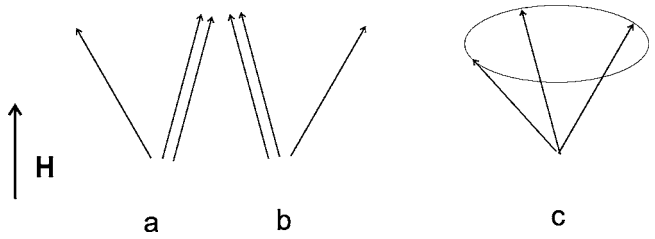

FIG. 13. Spin structures anticipated for the field just below the saturation point for $H \perp C^3$ (a and b) and for $H \| C^3$ (structure c).

survive in a broad temperature interval, characteristic for the wide critical range of low-dimensional systems.

The hysteresis observed in the magnetization curves of $RbFe(MoO_4)_2$ is most pronounced in the vicinity of the saturation field for $H \perp C^3$. This is probably due to the magnetocaloric effect which results in heating by a quickly rising magnetic field and cooling as the field is reduced. This magnetocaloric effect is due to the natural decrease of the entropy of the spin fluctuations in an applied magnetic field.

B. Resonance modes of the quasi-2D triangular antiferromagnet

The spin-resonance modes observed in high-frequency and high-field ranges are complementary to the previously published investigation.[10] As shown there, the observed ESR spectrum indicates the easy-plane character of the magnetic anisotropy in $RbFe(MoO_4)_2$. This conclusion is now confirmed by the observed hierarchy of the saturation fields: $H_{sat\|} < H_{sat\perp}$. The energy gap and the splitting of the upper branch observed in the present work correspond well to those reported in Ref. 10. Here, we observe the softening of the lowest magnetic-resonance branch in the saturation field. The field dependence of the electron-spin-resonance frequencies was calculated in Ref. 5 for a three sublattice model in the 2D molecular-field approximation. The results of these calculations are presented by a dashed line in Fig. 10. They agree qualitatively with observed resonance frequencies. These calculations do not include fluctuations resulting in the plateau; therefore the theoretical curves have singularities only in the magnetic field $\frac{1}{3}H_{sat}$ and not at the boundaries of the plateau range.

For the low-field region below 5 T, we performed the molecular-field calculations for the six sublattice model, taking into account the antiferromagnetic spin arrangement in the neighboring planes and following the model analogous to that of Ref. 17. The parameters used for these calculations are $6JS/(g\mu_B)=6$ T, $4J'S/(g\mu_B)=0.0425$ T, and $DS/(g\mu_B)=0.57$ T, where J and J' are the intralayer and interlayer exchange constants and D is the effective anisotropy constant of the model Hamiltonian given in Ref. 10. The resonance mode that appears at around 35 GHz and 3 T in Ref. 10 as well as the splitting of the upper branch noticeable in Fig. 8 are reproduced by this calculation. The value of $6JS/(g\mu_B)$ was taken from the saturation field expression[5] $g\mu_B H_{sat\|}=18JS$. The values of $DS/(g\mu_B)$ and $4J'S/(g\mu_B)$ are chosen to fit the observed antiferromagnetic-resonance gap, the splitting of the upper mode, and the frequency of an additional mode around 35 GHz.

The solid lines in Fig. 11 are calculated using the rigorous results of molecular-field calculations for the six sublattice model of a stacked triangular antiferromagnet[17] for $\mathbf{H}\|C^3$ with the same parameters as used above. Due to the easy-plane magnetic anisotropy of $RbFe(MoO_4)_2$, the umbrella-like spin structure should be valid in the whole magnetic-field range at $\mathbf{H}\|C^3$. In this case, we can use formulas (3.17)–(3.21) of Ref. 17. The agreement between experiment and this calculation is excellent.

Note that both the molecular-field approach using the six sublattice model and the macroscopic approach used in Refs. 10 and 11 are in good agreement. Both methods result in the following zero-field relation between the frequency of the exchange mode appearing due to the interplanar exchange and the splitting of the main mode of the antiferromagnetic resonance:

$$f_{2,3}^2 - f_{5,6}^2 = f_1^2/2. \tag{1}$$

Here, the frequencies f_i correspond to the magnetic-resonance modes indicated in the inset of Fig. 11. Both methods also predict the peculiar field dependence of the ESR frequency at $\mathbf{H}\|C^3$ with $\frac{df}{dH}$ being approximately a half of this value for free spins.

Magnetic-resonance frequencies enable one to determine several important values. First, the interplanar exchange integral J' (given above) is derived from the zero-field frequency of the spin-resonance mode noted as f_1 in Ref. 17 (ν_6 in Refs. 10 and 11):

$$f_1 = \frac{12\sqrt{JJ'}S}{2\pi\hbar}. \tag{2}$$

Further, from the observed AFM resonance gap of the intense modes, we can estimate the reduction of the magnetic-resonance frequency due to the zero-point fluctuations. We take $18JS/g\mu_B=18.2$ T from the measured saturation field $H_{sat\|}$. The difference between the saturation fields for the two field directions calculated in molecular-field approximation is

$$\mu_0(H_{sat\perp} - H_{sat\|}) = 2DS/(g\mu_B) \tag{3}$$

and results in the anisotropy field $DS/(g\mu_B)=0.85\pm0.15$ T. Thus, we predict in the molecular-field approximation the resonance frequency at zero field as $f_0=\sqrt{18JDS}/2\pi\hbar = 110\pm10$ GHz. Here, the g factor is 2.01 as measured in Ref. 14. The observed magnetic-resonance gap $f_0=90$ GHz is only 0.82 ± 0.08 of the predicted value. This deviation should be due to the reduction of the effective anisotropy and ordered spin component by zero-point fluctuations. According to Chubukov and Golosov,[5]

$$2\pi\hbar f_0 = \sqrt{18J\tilde{D}}S^*, \tag{4}$$

where $\tilde{D}$ is the renormalized anisotropy constant and S^* is the ordered spin component. The theoretical estimations based on $1/S$ expansion[5,18] are $\tilde{D}=D(1-1/2S)$ and $\frac{S^*}{S}\approx 1-0.26/S=0.90$. From here, we deduce the ratio of f_0 values, calculated by formula (4) and in molecular-field approximation as 0.80, which corresponds to the experimental value within the experimental error. The value of the reduction of the ordered spin component was measured in NMR experiments[16] in the magnetic field $\mu_0 H=5$ T; these measurements resulted in $\frac{S^*}{S}=0.87$, which is also in correspondence with the above theoretical estimations. However, it should be noted that the reduction of the ordered spin component should be field dependent, vanishing at the saturation field.

V. CONCLUSIONS

The complete phase diagram of a quasi-two-dimensional antiferromagnet with a regular triangular lattice is obtained. The peculiarity of the saturation process is the splitting of the transition from the ordered to a paramagnetic phase and a "delayed" saturation. The spin-flip mode of the antiferromagnetic resonance at the saturation field of an antiferromagnet with a "triangular" spin structure is found. The reduction of the antiferromagnetic-resonance gap due to zero-point fluctuations is ascertained.

ACKNOWLEDGMENTS

The authors are indebted to A. V. Chubukov, S. E. Korshunov, M. Lees, V. I. Marchenko, O. A. Petrenko, S. S. Sosin, L. E. Svistov, N. Wilson, and M. E. Zhitomirsky for discussions. This work was in part supported by the Grant-in-Aid for Scientific Research on Priority Areas from the Japanese Ministry of Education, Culture, Sports, Science and Technology and supported by the Russian Foundation for Basic Research Grant No. 07-02-00725. Some of these studies were done under a Foreign Visiting Professor Program in KYOKUGEN, Osaka University.

[1] H. Kawamura and S. Miyashita, J. Phys. Soc. Jpn. **53**, 4138 (1984).
[2] H. Kawamura and S. Miyashita, J. Phys. Soc. Jpn. **54**, 4530 (1985).
[3] D. H. Lee, J. D. Joannopoulos, J. W. Negele, and D. P. Landau, Phys. Rev. B **33**, 450 (1986).
[4] S. E. Korshunov, J. Phys. C **19**, 5927 (1986).
[5] A. V. Chubukov and D. I. Golosov, J. Phys.: Condens. Matter **3**, 69 (1991).
[6] N. Suzuki and F. Matsubara, Phys. Rev. B **55**, 12331 (1997).
[7] R. S. Gekht and I. N. Bondarenko, Zh. Eksp. Teor. Fiz. **111**, 627 (1997) [JETP **84**, 345 (1997)].
[8] M. F. Collins and O. A. Petrenko, Can. J. Phys. **75**, 605 (1997).
[9] T. Inami, Y. Ajiro, and T. Goto, J. Phys. Soc. Jpn. **65**, 2374 (1996).
[10] L. E. Svistov, A. I. Smirnov, L. A. Prozorova, O. A. Petrenko, L. N. Demianets, and A. Ya. Shapiro, Phys. Rev. B **67**, 094434 (2003).
[11] L. E. Svistov, A. I. Smirnov, L. A. Prozorova, O. A. Petrenko, L. N. Demianets, and A. Ya. Shapiro, Phys. Rev. B **74**, 139901(E) (2006).
[12] L. E. Svistov, A. I. Smirnov, L. A. Prozorova, O. A. Petrenko, A. Micheler, N. Büttgen, A. Ya. Shapiro, and L. N. Demianets, Phys. Rev. B **74**, 024412 (2006).
[13] G. A. Jorge, C. Capan, F. Ronning, M. Jame, M. Kenzelmann, G. Gasparovic, C. Broholm, A. Ya. Shapiro, and L. N. Demianets, Physica B **354**, 297 (2004).
[14] S. A. Klimin, M. N. Popova, B. N. Mavrin, P. H. M. van Loosdrecht, L. E. Svistov, A. I. Smirnov, L. A. Prozorova, H.-A. Krug von Nidda, Z. Seidov, A. Loidl, A. Ya. Shapiro, and L. N. Demianets, Phys. Rev. B **68**, 174408 (2003).
[15] G. Gasparovic, M. Kenzelmann, C. Broholm, S. Park, L. N. Demianets, and A. Ya. Shapiro, March Meeting of APS 2003 (unpublished), Session 31.
[16] L. E. Svistov, L. A. Prozorova, N. Büttgen, A. Ya. Shapiro, and L. N. Dem'yanets, JETP Lett. **81**, 102 (2005).
[17] H. Tanaka, S. Teraoka, E. Kakehashi, K. Iio, and K. Nagata, J. Phys. Soc. Jpn. **57**, 3979 (1988).
[18] A. V. Chubukov, S. Sachdev, and T. Senthil, J. Phys.: Condens. Matter **6**, 8891 (1994).